



# Geotechnical investigation and landslide susceptibility assessment along the Neelum road: a case study from Lesser Himalayas, Pakistan

Khawaja Shoaib Ahmed<sup>1</sup> · Muhammad Basharat<sup>1</sup> · Muhammad Tayyib Riaz<sup>1,2</sup> · Yasir Sarfraz<sup>1</sup> · Amir Shahzad<sup>1,2</sup>

Received: 22 October 2020 / Accepted: 21 May 2021 / Published online: 29 May 2021  
© Saudi Society for Geosciences 2021

## Abstract

Globally, and in Pakistan, among natural hazards, landslides are considered one of the most dangerous and frequently occurring events having devastating impacts on society and economy. The present study deals with the susceptibility mapping and detailed geological and geotechnical investigations on two large-scale landslides named Shahkot and Sandok, Lesser Himalayas, Pakistan. Inventory of 74 landslides was developed by SPOT-5 images and further classified in the field. The goodness of developed landslide susceptibility map was assessed by success rate curve (SRC) and prediction rate curve (PRC) which were 83.1% and 79.2%, respectively. Geotechnical investigations of selected landslides were carried out to identify the causative factors and landslide triggering mechanism. The Shahkot landslide is classified as complex (debris slide and slump failure), whereas the Sandok landslide is classified as rockslide. Laboratory testing, i.e., sieve analysis, Atterberg limits, specific gravity, and X-Ray Diffraction (XRD) analysis of the disturbed soil samples, reveal that the soils of Shahkot landslide are silty sand to clayey silty sand with plasticity index (PI) ranging from 2.05 to 14.96%. Petrographic studies showed that the schist and granite of the Shahkot and Sandok landslides contain quartz and feldspar with fair amounts of flaky minerals like chlorite, biotite, and muscovite. The XRD analysis showed mineral composition of quartz, muscovite, kaolinite, goethite, aragonite, hematite, plagioclase, siderite, montmorillonite, calcite, gypsum, orthoclase, dolomite, and illite. Intense jointing and fracturing in granite due to close proximity to faults imparts low unconfined compressive strength (UCS) values which holds the major cause of Sandok landslide beside other geomorphological and geological causes. The study depicts that drainage network, anthropogenic activities along steep slopes, fragile geology, active faults, freeze, and thaw action are influential parameters which significantly contribute to the landslide events.

**Keywords** Landslide susceptibility · Geotechnical investigations · Petrography · XRD · UCS

## Introduction

Natural hazards especially landslides are major challenges around the globe, and many countries are employing immense amount and resources to cope with them. In developing countries like Pakistan, landslide is among the major disasters responsible for fatalities, damages of the communication links, loss of fertile soil, and economic losses in the mountainous

areas (Petley et al. 2006; Jadoon et al. 2015; Owen et al. 2008; Kamp et al. 2008; Basharat 2012). Particularly, northern part of Azad Kashmir is characterized by steep slopes, active tectonics, fragile rock units, and heavy rains that result the area more susceptible to landslides. Strong earthquakes are among the prime triggering factors of landslides. On October 8, 2005, the Kashmir earthquake (Mw = 7.6, US Geological Survey) occurred on the NW–SE trending Kashmir Boundary Thrust (KBT), at the northwestern side of the Hazara Kashmir Syntaxis (HKS), northern Pakistan. The 2005 Kashmir earthquake triggered several thousands of landslides in the region.

Various methods and techniques have been applied for landslide susceptibility mapping, e.g., inventory-based methods (Akgun 2012), logistic regression (LR) statistical index, artificial neural networks (ANN), frequency ratio (FR), cluster analysis, weight of evidence (WoE) (Pradhan and Lee 2010; Yılmaz 2009; Buša et al. 2019; Riaz et al. 2018; Sujatha et al. 2012), analytic hierarchy process (AHP), fuzzy logic

---

Responsible Editor: Biswajeet Pradhan

✉ Muhammad Tayyib Riaz  
tayyibriaz@yahoo.com

<sup>1</sup> Institute of Geology, University of Azad Jammu and Kashmir  
Muzaffarabad, Muzaffarabad, Pakistan

<sup>2</sup> Department of Geology, University of Azad Jammu and Kashmir,  
Neelum Campus, Athmuqam, Pakistan

(Basharat et al. 2016; Leonardi et al. 2016; Vojteková and Vojtek 2020; Senouci et al. 2021), data mining, and machine learning (ML) methods (Ali et al. 2020; Lee et al. 2017; Kavzoglu et al. 2019; Al-Najjar and Pradhan 2020).

ML and statistical models are mainly affected by the causative factor selection (Feizizadeh et al. 2017; Can et al. 2019). However, the integrated models have been effectively used during last few years to improve the susceptibility (Kalantar et al. 2018). Several studies of model integration include ensemble models (Bragagnolo et al. 2020) and integration of knowledge-based and data-driven models (Zhang et al. 2019). In addition, Yilmaz and Ercanoglu (2019) addressed the importance of data mining selection techniques and experienced that polygon feature sampling methods are more realistic in attaining the reliable maps than other techniques.

After the Kashmir earthquake, various studies on coseismic landslide identification, distribution analysis, evolution, size, lithological control, and susceptibility mapping have been carried out in the area (e.g., Petley et al. 2006; Kumar et al. 2006; Sato et al. 2007; Dunning et al. 2007; Kamp et al. 2008; Owen et al. 2008; Khan et al. 2010; Saba et al. 2010; Chini et al. 2011; Basharat et al. 2014; Basharat et al. 2016; Shafique et al. 2016; Riaz et al. 2018; Riaz et al. 2019). However, few studies dealt with the geotechnical investigations of landslides (e.g., Kiyota et al. 2011; Konagai and Sattar 2012; Sattar et al. 2011; Riaz et al. 2019). They identified major landslides in terms of susceptibility and size in the region, i.e., Donga Kas and Hattian Bala landslides. Riaz et al. (2019) investigated the Donga Kas landslide to evaluate the possible initiation mechanism and movement. However, the remaining landslides (i.e., Sandok and Shahkot) needed to be investigated, so this study was an attempt to analyze the failure mechanisms of these catastrophic landslides. Unfortunately, no landslide susceptibility map is available along the studied road section which was the clear need to analyze the susceptibility in the region.

The study area lies in the Neelum valley situated towards the northeast of the Muzaffarabad and is part of the lesser Himalayan region. It is a steep, bow-shaped valley comprises of an area about 3621 Km<sup>2</sup> which hosts the total population of about 200,000 inhabitants (Planning and Development Department AJK 2015). The slope failures occur mainly along the main road built in the mountain environment. In addition, the deforestation has further enhanced the phenomenon of mass wasting in the region (Rieux et al. 2007). The road along Neelum valley is the main transportation corridor which connects Muzaffarabad, the capital city of Pakistani Administrated Kashmir (PAK), with the other localities of the Neelum valley. The road has been badly affected due to landslides during the rainy season and caused road blockage for many days to weeks. The blockage of this road often causes isolation of the population and shortage of food, medicine, and other commodities. The road has been blocked

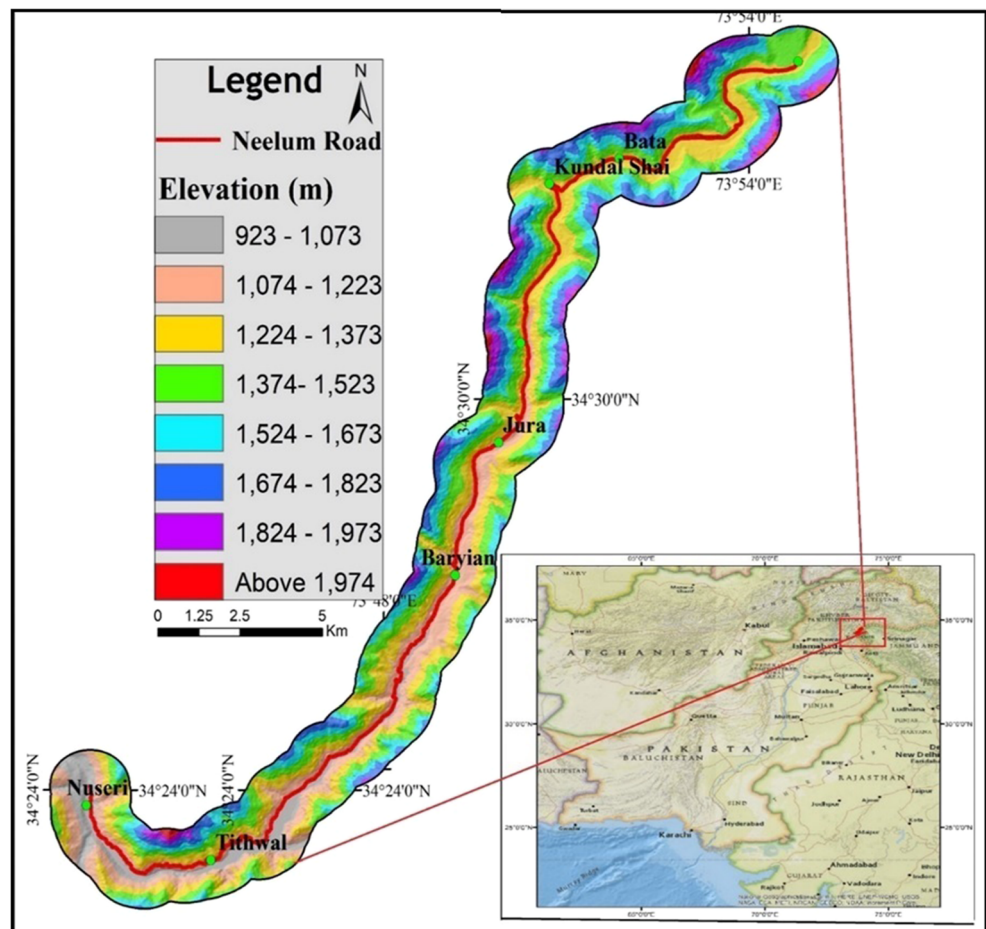
more than 45 days as a result of massive landsliding activated by the earthquake (Basharat et al. 2012; Basharat et al. 2017). Resultantly, the communication link was totally disrupted between Muzaffarabad and other parts of the Neelum Valley. In response, the relief and rescue operation during the earthquake was badly affected. These landslides caused the severe damage on landscape and road infrastructure. On the contrary, many other shallow landslides were also triggered during this earthquake and resulted in number of fatalities and severe damage to the main road.

There was a clear need and gap in the literature to investigate the landslide susceptibility and to analyze the geotechnical and mineralogical behavior of landslide material in the region. Therefore, the current study was carried out along road section from Nauseri to Athmuqam, district Neelum valley, Azad Kashmir, Pakistan, to fill out this gap (Fig. 1). Firstly, the landslide inventory of the area was prepared using SPOT-5 satellite imageries and was classified in the field too. Landslide probability map of the region by applying WoE method was developed to identify the probable hazardous zones. Two large-scale catastrophic landslides (Sandok and Shahkot) were selected for the detailed geotechnical and geomorphological investigation to comprehend the causes and failure mechanism (Fig. 1). The objectives of this study were to identify and characterize the landslide hazardous zones along Neelum Valley road that could help the planners and decision makers for the safe continuity of traffic along the main Neelum road in future. To minimize the landslide-associated risk in the future and to understand the landslide mechanism, this research focused on generating a susceptibility map and geotechnical investigation. This study is the first attempt to understand the primary root cause of landslide mechanism by integrating geotechnical, mineralogical, and remote sensing-based approach in the region and will contribute as primary database for future research in this domain.

## Geology and tectonics of the study area

The study area is generally mountainous with narrow valleys. The altitude ranges between 923 and 1974 m asl (Fig. 1). The steep slopes and escarpments are prominent features of the area. The Neelum River and its tributaries drain the entire region. Tectonically, the study area is part of the NW Himalayan fold and thrust belt (Kazmi and Jan 1997). The area lies primarily in the eastern side of the HKS, Lesser Himalayas, across the Main Boundary Thrust (MBT). The MBT, Panjal Thrust (PT) and local faults, i.e., Barian Fault, Islampura Fault, and Bata Fault, are present within the study area (Fig. 2). The Panjal Formation is thrust over the Muree Formation of Miocene age along the MBT (Khan 1994). The PT marks the boundary between the Tanol Formation of

**Fig. 1** Geographical location of the study area



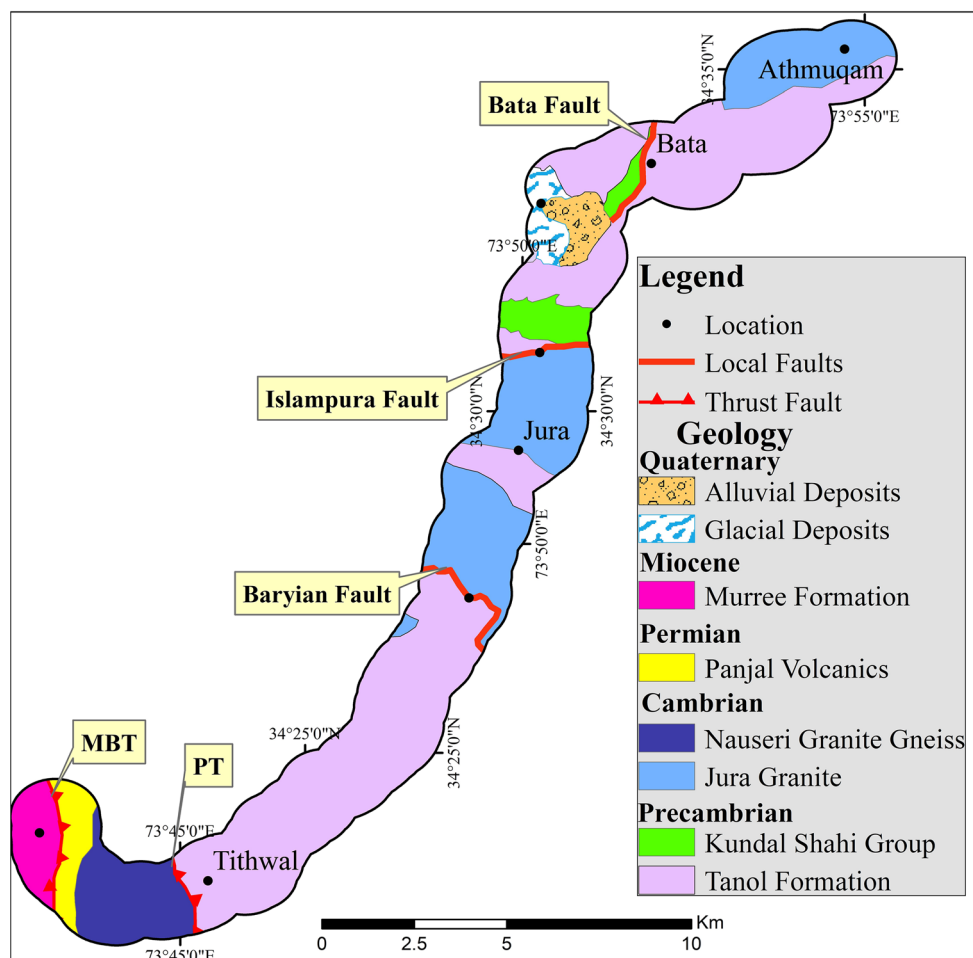
Precambrian age and the Panjal Formation of the Carboniferous-Triassic age at the eastern limb of the HKS. The Cambrian Neelum/Jura granite is intruded in the Tanol Formation. Barian Fault lies between the Tanol schist and the Jura granite and dips to the northeast at about  $30^\circ$ . The fault lies towards south of the Sandok landslide and effect of shearing is prominent along this fault. The northern contact of granite exposed in Sandok landslide is also faulted which is exposed at the opposite side on the left bank of the Neelum river near Islampura village. The Bata Fault is exposed towards the southern end of the Shahkot landslide and lies between Athmuqam biotite chlorite schist-phyllite and the Kundalshahi Nagdar garnet mica schist (Ghazanfar et al. 1983).

Rocks of Lesser Himalayas comprises the Tanol Formation of Precambrian age, intruded by the Mansehra type granites of the Cambrian (Wadia 1931; Calkins et al. 1975; Fig. 2). Precambrian Tanol Formation generally comprises of meta-sediments including quartzose schist, chlorite schist, graphitic schist, garnet mica schist, and quartzite. The Tanol Formation is intruded by the Jura granite of the Cambrian age and further intruded by dolerite dykes. The general dip direction from Sandok to Shahkot village is northeast (Ghazanfar et al. 1983).

## Methodology

The data related to landslide hazards along the Neelum road in general and about the landslides problem in particular was limited. However, all the available information was gathered and used. Landslide inventory map of the area was prepared by utilizing SPOT-5 satellite imageries and Google earth and further classified in the field in accordance to Varnes (1978) classification. Landslide causative factors were identified, and eight causative factor maps were prepared. Digital elevation model (DEM) of 12.5m resolution was utilized for computation of slope, aspect, curvature, elevation, and drainage network causative factor rasters in Arc-GIS 10.8 environment. Landslide polygons were converted to point features and randomly subdivided into (70:30) training and validation samples by utilizing subset features tool in Arc-GIS. Geological map and fault network were digitized from existing maps and then rasterized. A data-driven WoE method was adopted to generate the susceptibility map of the area. Arc-SDM tool was used for computation of weights and other calculations. Developed landslide susceptibility map was validated by SRC and PRC curves. Based on developed susceptibility map, the study region was classified to low susceptible,

**Fig. 2** Geological map of the study area



moderate susceptible, high susceptible, and very high susceptible zones. Methodological steps for generating susceptibility maps are similar as Riaz et al. (2018).

Detailed geotechnical and geochemical investigations were also carried out. Furthermore, base map of each landslide was prepared for detail geotechnical mapping and construction of profiles. For this purpose, longitudinal and cross-sectional profiles have been constructed. The profiles basically show the initiation of landslide movement and related material exposed on the landslide body. These profiles have been used to understand the relationship between the intact mass and the material moved along the failure surfaces. The volume of landslides was roughly assessed by multiplying the landslide deposit area with the average thickness (Basharat et al. 2012). The field investigations were carried out using Laser Distance Meter (RIEGL-F-21H), Clinometer, Global Positioning System (GPS), Brunton, and tape measurements. Two major landslides, i.e., Shahkot and Sandok, have been mapped on scale 1:6000 and 1:1000 respectively by using ArcGIS software. The various lithological units have been observed and mapped. The rock and disturbed soil samples have been taken for soil classification and to identify the shear

strength parameters of the failure zones. The samples were taken systematically from main scarp, main body, and toe areas, three samples from each segment, i.e., right flank, middle portion, and left flank. A total of 11 soil samples and 12 rock samples were collected according to the material exposed along the sliding surfaces. The 5kg soil samples were collected with the help of auger from 1 m depth and were packed in air tight plastic bags to avoid loss of moisture content.

A series of laboratory tests such as grain size distribution, Atterberg limits, specific gravity, UCS, petrography, and XRD were performed on disturbed soil samples and rock core samples to determine the strength and physical characteristics of the material for slope failure. These tests have been performed according to the American Society for Testing and Materials (ASTM) standard test methods. Grain size analysis was performed according to ASTM D422 standard using standard set of sieves. Atterberg limits were determined by ASTM D4318-00 standard test method which include liquid limit by Casagrande's one-point method and plastic limit by using glass plate. ASTM standard test method D854-14 was used to determine the specific gravity by Pycnometer. UCS test was



performed using ASTM D7012-14e1. Twelve core samples were cut to required dimensions, grinded to make the surfaces smooth, and then tested to determine the UCS of each sample. For petrographic analysis, thin sections were prepared and studied under petrographic microscope according to ASTM C295/C295M-19. XRD was performed on powdered samples in the Geoscience Laboratory of Geological Survey of Pakistan, Islamabad.

## Results and discussions

### Landslide inventory

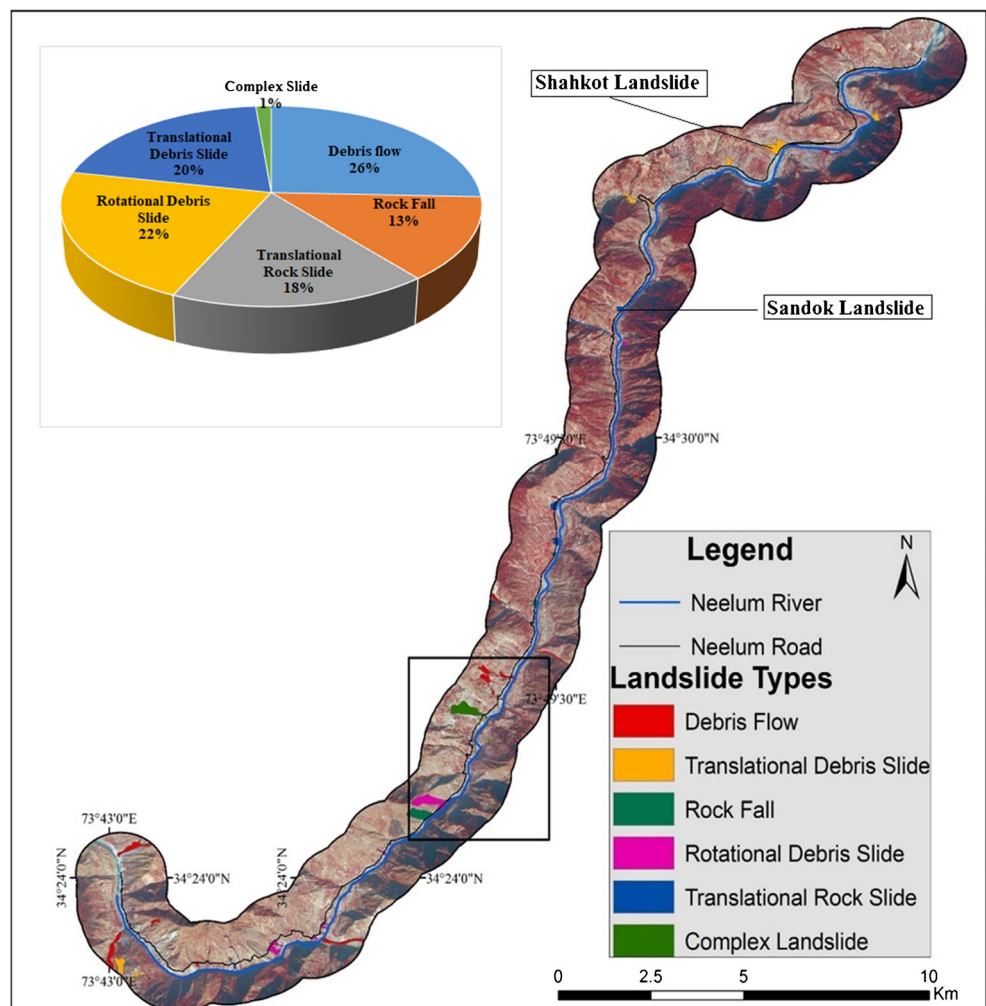
The classification system used for this study is based on Varnes (1978). To classify the landslides along the Neelum Valley road, the terminology approved in the literature was used. Seventy-four landslides were observed and demarcated via SPOT-5 and classified during field investigations. Based on field observation, these landslides were classified as debris

flow, rotational debris slide, translational slide, rock fall, complex, and rockslides (Fig. 3). Majority of the landslides are debris flow (26%), followed by rotational debris slide (22%), translational debris slide (20%), translational rockslides (18%), rock fall (13%), and complex slide (1%).

### Landslide causative factors

The landslide probability was evaluated by integrating existing landslide locations with evidential rasters. Eight causative factors including topographic factors (slope aspect, slope gradient, curvature, drainage network, and elevation), geological factors (lithology and fault lines), and road network were derived (Fig. 4). These parameters were considered as causative factors for the slope failure in the study area. These all 8 causative factors were processed in raster in ArcGIS. Slope gradient ascertains the divergence and convergence of rainwater on a slope and thereby affects soil formation, soil water content, slope stability, and erosion potential (Vijith and Madhu 2008).

Fig. 3 Landslide inventory of the area



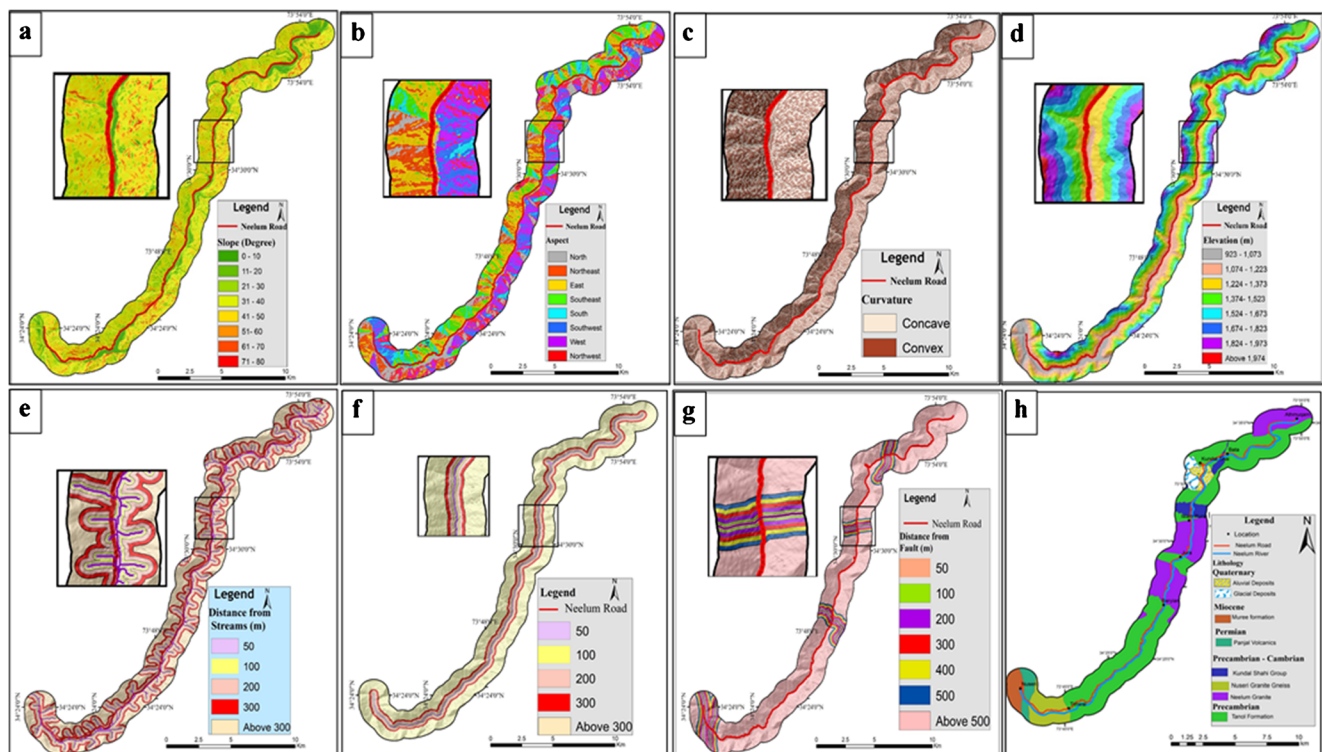


**Fig. 4** Landslide susceptibility causative factors: **a** slope gradient; **b** slope aspect; **c** curvature; **d** terrain elevation; **e** distance to streams; **f** distance to road; **g** distance to faults; **h** lithological units

Slope aspect is another important contributing factor, e.g., slope directly faces the hitting of the sun light resulting in the melting of snow and water infiltration, which increases the freezing and thawing action, due to which slope failure occurs. Slope failure is also affected by curvature (Nefeslioglu et al. 2008). Elevation is a dominant contributory factor considered for landslide probability mapping (Dai and Lee 2001). Lithological units are one of the more important contributing parameters for landslide distribution (Yalcin 2008). Loose and fragile lithological units are more prone to landslides (Kamp et al. 2008). Fault rupture and geometry have direct impact on the occurrence of landslides (Mahmood et al. 2015). Road construction activities, e.g., blasting, excavation, undercutting, and heavy traffic vibrations are also responsible for landslides (Mittal et al. 2008). According to Dahal et al. (2008), undercutting and toe erosion due to stream network are considered as significant contributing parameters for landslides.

### Landslide susceptibility mapping

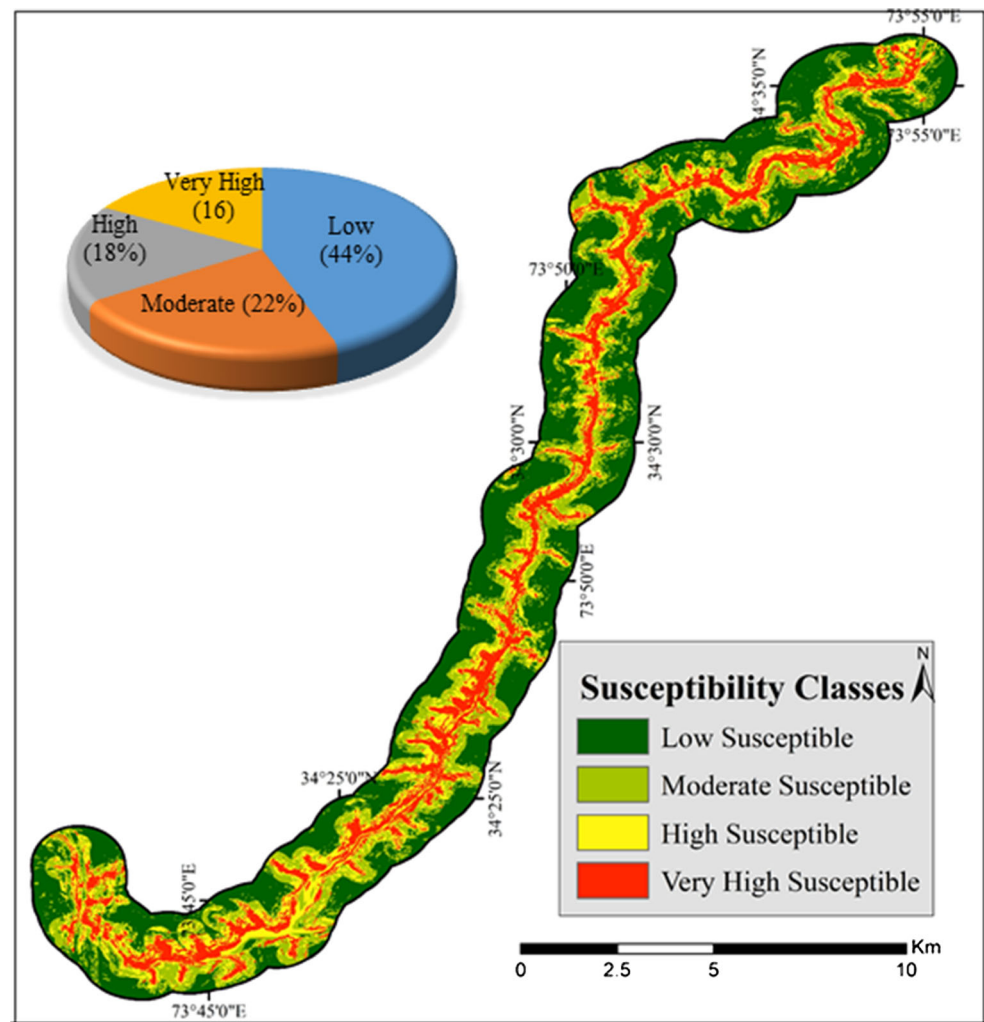
The probability of occurring a landslide in the area based on local terrain environment fell under the definition of landslide susceptibility (Brabb 1984; Fell et al. 2008). Probability assessment starts with valid landslide inventory, evidential parameters selection, and computation of appropriate approach to analyze the contribution of controlling factors on landslide distribution (Fell et al. 2008; Van Westen et al. 1997). Various

methods for landslide probability mapping depend on the data accessibility and local ground settings.

Different quantitative and qualitative methods are developed for landslide probability analysis (e.g., Aleotti and Chowdhury 1999; Guzzetti et al. 2005; Soeters and van Westen 1996). In this research, we adopted data-driven WoE method for landslide probability mapping (Fig. 5). The WoE works by allocating weights to each class of the thematic parameter, based on spatial association to that parameter and identified landslide locations. Bayesian approach was employed in WoE to ascertain the impact of the spatial association between landslide locations and classes of evidential factors to compute weights.

To evaluate and investigate the association of each evidential factor with landslides, a set of tables were generated by the Calculate Weights tool in Arc-SDM (Table 1). The analysis of slope gradient evidential theme showed the slope class (61–70°) has highest weight (2.336) and has positive correlation with landslides, while the least weight value is generated by slope class (0–10°) which is (–2.861). These values indicate the strong association between landslide points and slope classes. The analysis of weight tables for slope aspect indicates that higher weight value obtains by east-facing slope which is 0.705 followed by south-facing slope which is 0.522. The minimum weight value is yielded by southwest-facing slope (–0.898). The weights for curvature causative factor revealed that the maximum weight value was assigned to concave

**Fig. 5** Developed landslide susceptibility map of the area



curvature which is 0.220. While the lowest weight value is for convex curvature which is  $-0.168$ .

The analysis of weights for elevation shows that maximum weight value is 1.013 which is at elevation class 1074–1223 m covered an area of 11.094 km<sup>2</sup> having 13 landslide points, while the lowest weight value is  $-2.538$  at elevation ranges from 1524 to 1673 m. This analysis of geological units reveals that highest weight value is of Panjal volcanics which is 1.145. This reveals that this class is most susceptible to landsliding. In contrast, lowest contrast value is of alluvial deposit which is  $-0.076$ . These results indicate that there is a strong association between landslides and lithological units. The weight analysis of distance to fault causative factor indicate that maximum weight value was yielded by the class 0–50 m which is 1.139, while lowest contrast value was obtained by the class 301–400 m which is  $-1.299$  having zero landslide points. These outcomes indicate that faults have great effect in triggering landslides.

The weight analysis of distance to drainage discloses that class 0–50 m computed the highest weight value which is 2.866 while the lowest weight value is of the class  $> 300$  m

which is  $-3.258$ . We concluded from these results that drainage is also another important causative factor for landsliding phenomenon. Distance to road is our last evidential theme and classified into five classes using Euclidean distances. The results of weights table show that highest weight value is of 0.705 which is the class of 0–50 m while the lowest weight value is  $-0.302$  which is for class 200–300 m indicating no positive association between training points and this class of evidential theme.

In this study, all the causative factors along with their calculated weights were combined in Arc-SDM tool to develop the susceptibility map. The developed probability map was then classified into low, moderate, high, and very high susceptible zone using cumulative area posterior probability curve (CAPP). The validation of the susceptibility map was carried out by SRC and PRC curves. The susceptibility map has 83% (SRC) and 79% (PRC) which is good enough for 76.6 km<sup>2</sup> of the area (Fig. 6). Overall, 44% of the area fall under low susceptible zone, 22% in moderate susceptible zone, 18% in high susceptible zone, while 16% of the area fall in very high susceptible zone.

**Table 1** Weights of each factor estimated by weights-of-evidence considered in this study

Causative factors	Classes	Landslide points	W+	W-	Contrast (C)	Weight	Weight STD
Slope (degree)	0–10	1	-2.861	0.052	-2.914	-2.861	1.004
	11–20	2	-1.590	0.149	-1.739	-1.590	0.306
	21–30	7	-0.443	0.186	-0.538	-0.443	0.435
	31–40	9	-0.841	0.204	-1.219	-0.841	0.349
	41–50	10	-0.897	0.175	-0.933	-0.875	0.779
	51–60	11	-0.443	0.186	-0.538	-0.443	0.435
	61–70	12	2.336	0.184	2.530	2.336	0.794
Slope aspect	North	5	0.132	0.180	-0.340	-0.302	0.525
	Northeast	5	0.127	0.179	-1.424	-0.127	0.538
	East	14	0.709	0.194	0.876	0.705	0.381
	Southeast	10	0.474	0.187	0.560	0.474	0.427
	South	6	0.522	0.179	0.574	0.522	0.557
	Southwest	3	0.892	0.178	-0.991	-0.898	0.634
	West	5	0.577	0.182	-0.664	-0.577	0.507
Curvature	Northwest	4	0.498	0.179	-0.553	-0.498	0.572
	Concave	25	0.220	-0.168	0.389	0.220	0.256
	Convex	27	-0.168	0.220	-0.389	-0.168	0.230
Elevation (m)	923–1073	10	-0.897	0.175	-0.933	-0.875	0.779
	1074–1223	13	1.013	-0.193	1.205	1.013	0.430
	1224–1373	19	0.676	0.249	0.926	0.676	0.325
	1374–1523	9	-0.388	0.143	-0.493	-0.388	0.387
	1524–1673	1	-2.538	0.259	-2.798	-2.538	1.020
	1674–1823	0	0	0	0	-0.215	0.379
	1824–1973	0	0	0	0	-0.215	0.379
	Above 1974	0	0	0	0	-0.215	0.379
Lithology	Tonal Formation	31	0.167	-0.201	0.365	0.136	0.227
	Neelum granite	7	-0.767	0.196	-0.958	-0.762	0.420
	Kundulshahi group	2	0.040	-0.001	0.045	-0.064	0.498
	Glacial deposits	1	-0.217	0.004	-0.221	-0.064	0.496
	Alluvial deposit	1	-0.258	0.005	-0.258	-0.076	0.489
	Nauseri granite	5	0.408	-0.035	0.443	0.488	0.595
	Panjtal volcanic	3	1.043	-0.040	1.186	1.145	0.932
	Murree Formation	2	0.032	-0.009	0.024	-0.046	0.496
Distance to faults (m)	0–50	4	1.139	-0.026	1.153	1.139	1.141
	51–100	3	0.558	-0.258	0.813	0.558	0.794
	101–200	2	0.040	-0.001	0.045	-0.064	0.498
	201–300	1	-0.851	0.026	1.117	-0.851	1.103
	301–400	0	0	0	0	-1.299	1.067
	401–500	1	0.600	0.016	1.144	-0.600	1.131
	Above 500	41	0.051	-0.241	0.458	0.051	0.187
Distance to drainage (m)	0–50	21	2.866	-0.157	2.380	2.866	1.792
	50–100	12	1.319	-0.198	1.581	1.319	0.492
	100–200	10	-0.206	0.056	-0.262	-0.206	0.376
	200–300	8	-0.256	0.054	-0.310	-2.256	0.414
	Above 300	1	-3.258	0.673	-3.932	-3.258	1.009
Distance to road (m)	50–100	14	0.705	-0.170	0.876	0.705	0.538
	100–200	5	-0.127	0.014	-0.142	-0.127	0.525
	200–300	5	-0.302	0.383	0.340	-0.302	0.381
	300–400	10	0.476	-0.086	0.560	0.474	0.427
	Above 300	6	0.525	-0.051	0.574	0.525	0.557

## Field investigation, geotechnical mapping, and construction of profiles

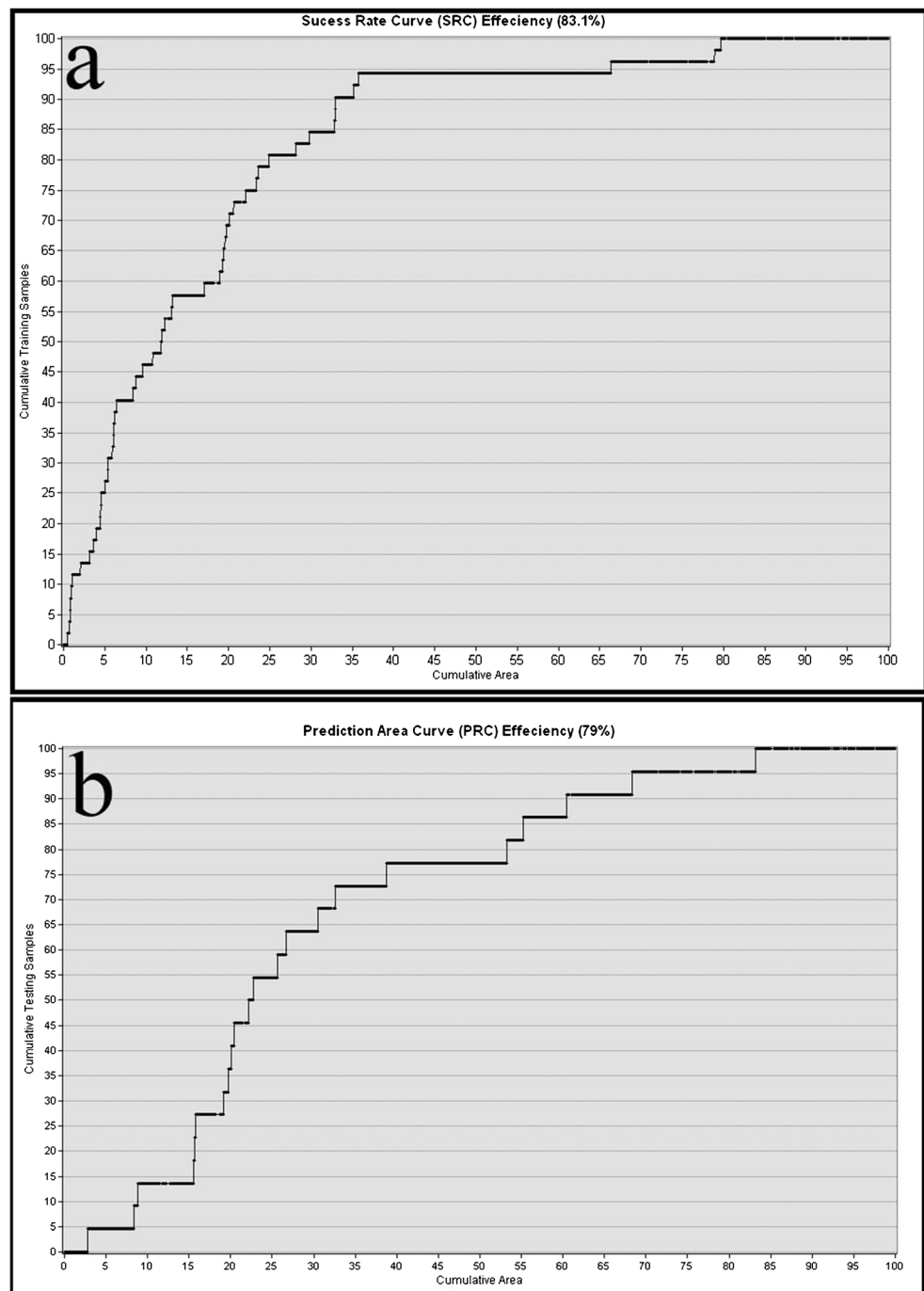
The discrete geological units of the investigated landslides have been recognized and mapped. The lithological units and geological formations have also been presented on the maps with bedding attitude where available.

## Shahkot landslide

The Shahkot landslide is situated about 72 Km North of Muzaffarabad alongside Neelum road, district Neelum Valley, Azad Kashmir. According to the native people, the Shahkot landslide was activated first time due to heavy flood in river Neelum in 1992. The landslide area was composed of



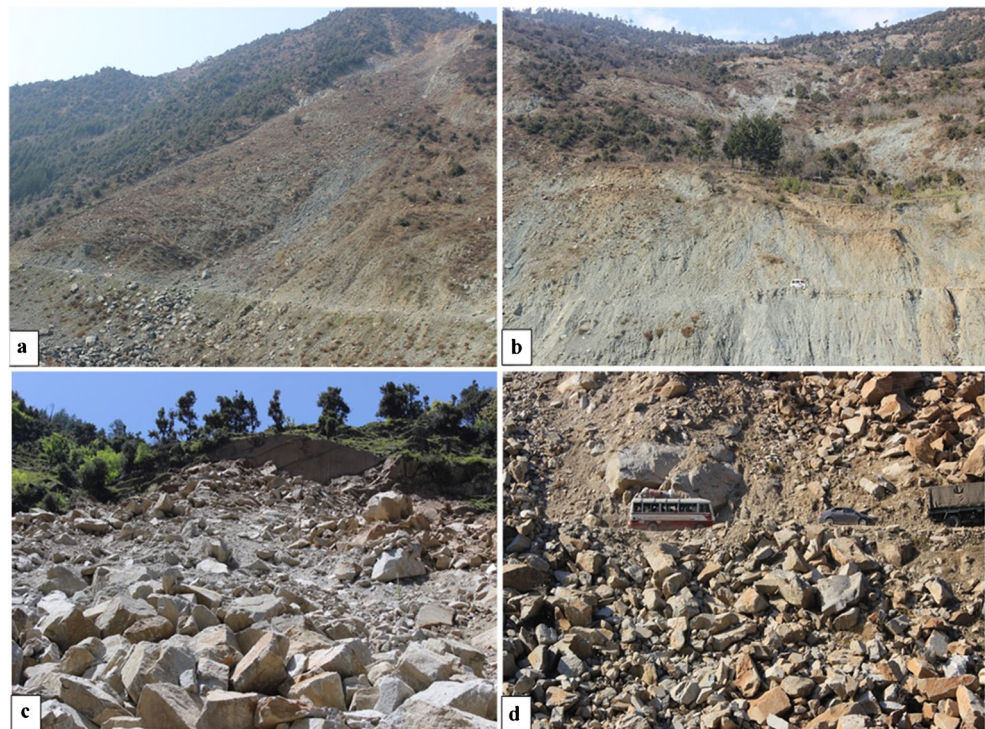
**Fig. 6** Landslide susceptibility validation curves: **a** success rate curve (SRC); **b** prediction rate curve (PRC)



cultivated terraces with irrigation channels. These terraces and irrigation channels were destroyed due to the landslide. Consequently, the cultivation in adjacent area downstream was also abandoned. About 490m road section has been damaged by the landslide and caused disruption to the continuity of the traffic along this road (Fig. 7a, b). The landslide occurs within the meta-sediments of the Tanol Formation which comprises mainly of quartzose schist, garnetiferous chlorite mica schist, graphitic schist, quartzite bands, phyllite, and

schistose conglomerate. The scarp on the right flank consists of chlorite schist, graphitic schist, and phyllite of the Tanol Formation, while towards the middle and left flank, the detachment surface consists of clays, sub-phyllite, and schist debris (Fig. 8d). Thick vegetation cover is present above the crown and along the flanks as well as within the slumped material in the middle portion (Fig. 7a, b). Several seepages were also observed near the main scarp on the right flank and near the bottom of the main body on the left flank along the

**Fig. 7** Field photographs: **a** Shahkot landslide; **b** disturbed road through landslide material; **c** exposed scarp and landslide material of the Sandok landslide; **d** huge displaced material along the Sandok landslide



road. The landslide activity here relates to steepness of slope, presence of swelling clays and non-cohesive soils, river under cutting, and deforestation.

The zone of depletion of landslide on the right flank shows rock and debris slide and toppling, while along the middle portion and left flank, it shows slump movement with slightly curved surface. The measurement of the depletion zone of the landslide is variable along the circumference of the main scarp. On the right flank, it is 15–190 m wide and 85–150 m long, while on the left flank, it is about 10–190 m wide and about 90 m long (Fig. 8c). The exposed area of the zone is 32,300 m<sup>2</sup>. The sandy, silty, and clayey material is deposited in the depletion zone with coarse, platy fragments of schist, and sub-phyllite.

The transitional zone extends in length from 35–230 m and is 340–350 m in width (Fig. 8c). Area covered by the transition zone of landslide is 32,880 m<sup>2</sup>. The slope angle varies from 30° to 70° (Fig. 9a, c). The zone is considered as sandy zone with abundant gravel and pebble fraction. The main body of the landslide consists of clays, sand, gravel, and cobble fractions. The thick deposit of loose material along the traveling path enlarged the volume of the landslide. In the lower portion of the slide, the displaced material measures about 10–12 m above the road. The thickness of debris material is more below the road due to the dumping of material while clearance of the road from landslide material. The vegetation cover is also present within the transition zone towards the left flank where the landslide shows slump failure down-slope. The accumulation zone covers an area of 46830 m<sup>2</sup>.

The length of this zone is 100–180 m and the width is 350–365 m. It consists mainly of mixed debris material with some boulders and slabs. The toe area on the right flank of the landslide is categorized by debris flow with well-developed fan adjacent to the river. The length and width of the landslide are 650 m and 350 m, respectively. The thickness of the material is about 90 m and the estimated volume of the landslide is  $1.35 \times 10^7$  m<sup>3</sup>.

### Sandok landslide

The Sandok landslide is located approximately 65 Km north of the Muzaffarabad, alongside Neelum valley road, Azad Kashmir. The elevation varies from 1291 m at bottom to 1391 m at the top. This landslide was activated in year 2013 due to heavy and consistent rain fall for many days and initiates with huge mass towards the Neelum river. Resultantly, the river was completely blocked for a while, and the water level rose to approach the nearby village of Islampura. The blockage was then cleared through blasting. About 115m road section has been damaged by the landslide which disrupted the continuity of traffic along this road (Fig. 7c, d). Considering the aforementioned problems, the landslide was studied and mapped on a scale 1:1000 to know the reasons and the failure mechanisms (Fig. 8a, b). The Sandok landslide occurs in the granite intruded into the Tanol Formation. The rocks exposed along landslide and adjacent areas are highly jointed and cracked. The landslide material is displaced from

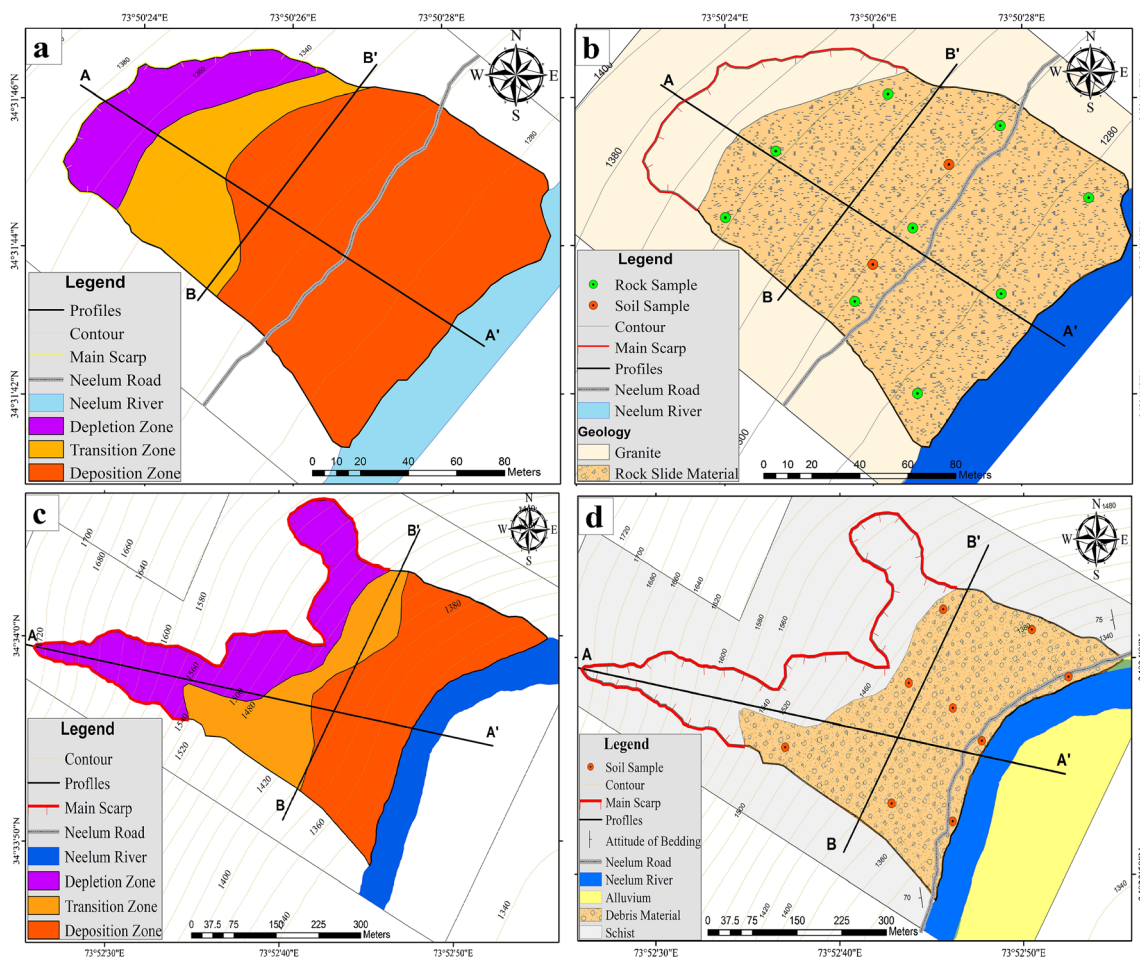


**Fig. 8** a Morphological map of the Sandok landslide; b geotechnical map of the Sandok landslide; c morphological map of the Shahkot landslide; d geotechnical map of the Shahkot landslide

the crown to toe. However, huge material is remained along the sliding surface.

The depletion zone of the Sandok landslide is 50–80 m wide and 10–15 m long (Fig. 8a). The main scarp is nearly vertical and extends about 15 m from the top of the slide. The total area of depletion zone is about 1250 m<sup>2</sup>. The scarp seems to have been formed due to detachment of blocks of granite along the nearly vertical jointed surface. The boulders of granite are stacked along the slope which may slide or topple as the landslide may reactivate. The rock mass in source area is highly jointed and fractured granite body. The vertical elevation from crown to toe is about 125 m. The absolute horizontal distance is calculated about 150 m. The accumulation of large boulders (several meters in diameter) with some unconsolidated material along down slope has increased the volume of landslide (Fig. 7c). The transition zone of the Sandok landslide consists mainly of overhanging boulders of granite. The transitional zone extends from 15–45 m in length and 70–95 m in width (Fig. 8a). Area covered by the transition zone of landslide is 3060 m<sup>2</sup>. Average thickness is measured about 6–8 m. The slope angle in this zone ranges from 40 to 70° (Fig.

9b, d). The deposition zone of the Sandok landslide is 75–100 m long and 100–115 m wide. The calculated surface area of deposition zone is 9440 m<sup>2</sup>. The zone of accumulation of the slide consists of large blocks and boulders of granite. Evidences of blasting were observed which was done to clear the Neelum road which may have further accelerated the rockslide. The diameter of the boulders ranges up to 5 m in diameter. Total volume is calculated about 0.11 million m<sup>3</sup> estimated by multiplying the average thickness with the covered area. The Neelum road runs through deposition zone of the landslide.

### Laboratory tests

#### Grain size distribution

The representative soil sample was obtained from the bulk soil sample by reducing the sample through quartering. The soil sample was then placed in the sieve shaker in ascending order. The mass of the material retained on each sieve was recorded. The quantity of the soil is based on the maximum particle size



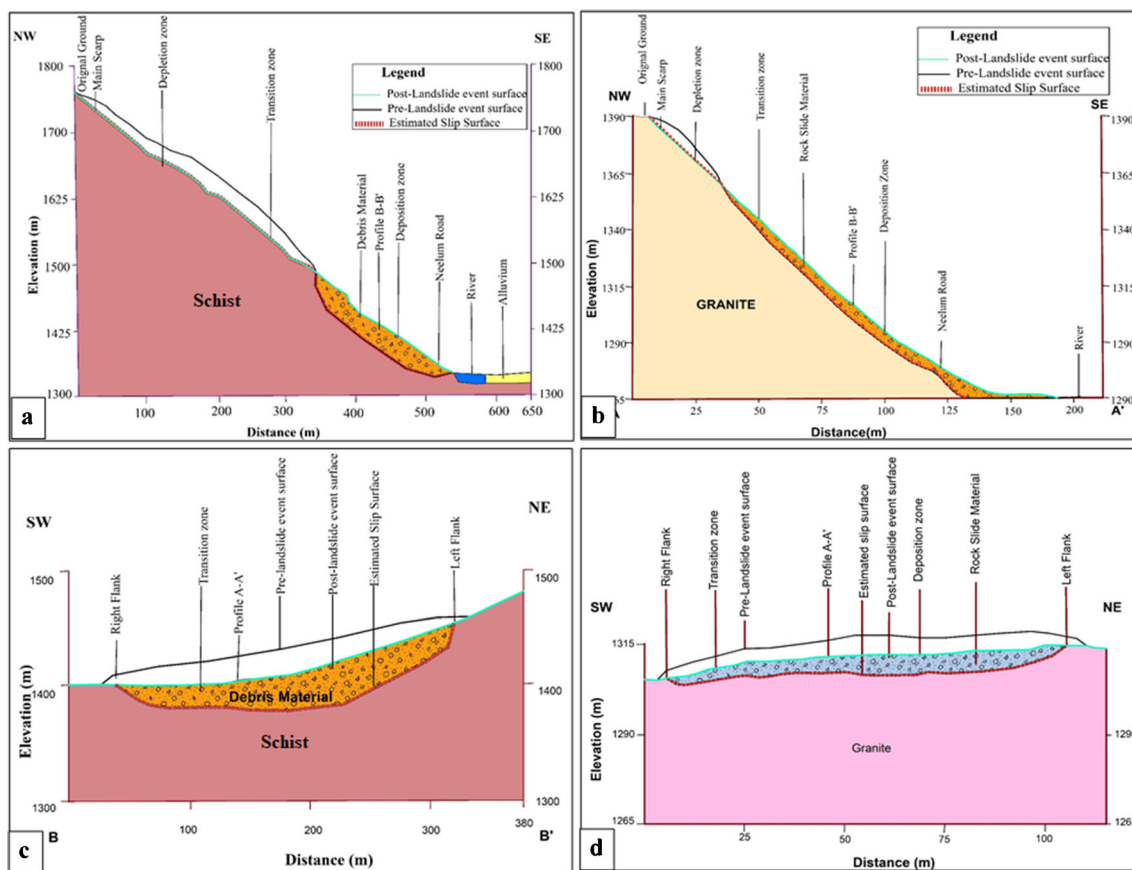


**Fig. 9** Landslide profiles: **a** longitudinal profile of the Shahkot landslide; **b** longitudinal profile of the Sandok landslide; **c** cross profile of the Shahkot landslide; **d** cross profile of the Sandok landslide

present in the soil. Retained percentage of soil samples of the Shahkot landslide from the depletion zone on sieve no. 4 is 38.2–54.6%, on sieve no. 50 is 89.9–90.6%, on sieve no. 100 is 95.9–96.2%, and on sieve no. 200 is 97.8–98.7%. Based on these results, the soil from the accumulation zone at right flank is classified as silty sand (non-cohesive). Retained percentage of soil from the accumulation zone at right flank and left flank on sieve no. 4 is 33–36%, on sieve no. 50 is 79.6–89%, on sieve no. 100 is 85–93.4%, and on sieve no. 200 is 93–97%. Based on these results, the soil from accumulation zone at right and left flank is classified as clayey silty sand (non-cohesive). Retained percentage of soil from accumulation zone at middle portion on sieve no. 4 is 44.3%, on sieve no. 50 is 88.3%, on sieve no. 100 is 96.2%, and on sieve no. 200 is 97.8%. Based on these results, the soil from accumulation zone at middle is classified as sandy silt (non-plastic). Retained percentage of soil of the toe area of accumulation zone on sieve no. 4 is 46.7–48.5%, on sieve no. 50 is 85.7–88.8%, on sieve no. 100 is 91.3–94.4%, and on sieve no. 200 is 96–97.6%. Based on these results, the soil from depletion zone is classified as clayey sandy silt (non-cohesive). Based on grain size distribution analysis, it is classified that the soils of transitional and accumulation zones are silty clayey sands

which holds the major failure along the slope due to the water seepages within the landslide body.

Retained percentage of soil sample of the Sandok landslide from accumulation zone at right flank on sieve no. 4 is 12.2%, on sieve no. 50 is 72.4%, on sieve no. 100 is 85.4%, and on sieve no. 200 is 93.6%. Based on these results, the soil from accumulation zone at right flank is classified as clayey silty sand (non-cohesive). Retained percentage of soil of accumulation zone at left flank on sieve no. 4 is 38.3%, on sieve no. 50 is 78.5%, on sieve no. 100 is 86.9%, and on sieve no. 200 is 91.4%. On the basis of these results, the soil from accumulation zone at left flank is classified as silty clayey sand (non-cohesive). Based on grain size distribution analysis, it is classified that the soils of transitional and accumulation zones are silty clayey sands.

#### Atterberg limits and plasticity index of soils

The liquid limit (LL), plastic limit (PL), and plasticity index (PI) of soils are also used extensively, either individually or together, with other soil properties to correlate with engineering behavior such as compressibility, hydraulic conductivity (permeability), compactibility, shrink-swell, and shear



strength. Fine soils (i.e., finer than 425  $\mu\text{m}$ ) are tested according to the ASTM standard D 4318–00. LL of Shahkot landslide soil samples ranges from 37.05 to 23.9%, PL ranges from 28.57 to 21.75%, and PI ranges from 14.96 to 2.15% that indicates the landslide material has high swelling potential (Table 2), whereas the LL of Sandok landslide soil samples ranges from 38.09 to 27.9%, PL ranges from 33.06 to 24.78%, and PI ranges 6.48 to 2.74 which indicates that the finer landslide material has slightly plastic behavior (Table 2).

### Specific gravity

To understand the physical characteristics of the landslide material, samples for specific gravity test were collected from top, middle, and base which were tested according to ASTM standard test method D854-14 and test results are presented in (Table 2). The specific gravity of the soil samples taken from the Shahkot landslide ranges from 2.72 to 2.33. The specific gravity of the soil samples taken from the Sandok landslide ranges from 2.71 to 2.53. These results indicate that the landslide body contains coarse grain materials.

### Unconfined compressive strength (UCS) of rock cores

UCS test was performed using ASTM D7012-14e1. A total of 12 samples were collected from the top, middle, and base of both the landslides. Three samples were collected from garnetiferous chlorite mica schist of the Tanol Formation in Shahkot landslide and 9 samples were collected from the Jura granite in Sandok landslide given in (Table 3). Shahkot landslide sample UCS test values range from 16.05 to 26.45 MPa which indicate very low compressive strength. The Sandok landslide sample UCS tests values range from 36.22 to 50.80 MPa which also indicate low compressive strength. The low values of the UCS in granite of the Sandok landslide

relates to the fact that the rock is highly fractured as observed in field as well as in petrography. The intensive fracturing of the rock unit is attributed to the presence of localized thrust faults in the vicinity of the landslide. The shearing strength of granite was overcome by the overburden pressure which causes the major failure along the slope. The very low UCS values of the Tanol schist in the Shahkot landslide correspond to the presence of flaky minerals like chlorite, micas, and other clay minerals observed in XRD and petrography which reduce the strength of the rock unit. Moreover, UCS was performed on the core samples oriented parallel to the shistosity planes due the fact that the direction of landslide failure plane also corresponds to the shistosity planes (Fig. 10).

## Petrography of exposed rocks in landslides

### Tanol Formation at Shahkot landslide

Three samples from the Shahkot landslide were collected for the petrographic study (SH-1, 2, and 3) from the Tanol formation exposed along the right flank of the landslide. In hand specimen, the fresh color of schist is greenish grey to light grey except few dark grey graphitic bands at places. The rocks are soft, fine grained, easily scratched with knife, and have low shistosity. Petrographic studies show that it contains subhedral to euhedral quartz with fair amount of flaky minerals like chlorite, biotite, and muscovite. Minor amount of garnet and other opaque minerals is also present. Mineralogically, the schist is composed of quartz 40–50%, muscovite 15–20%, chlorite 10–15%, opaque minerals 5–10%, and clay minerals 5–10% (Fig. 11a).

### Granite at Sandok landslide

Three samples were collected from the Sandok landslide for the petrographic study (SD-1, 2, and 3) from the Jura granite.

**Table 2** Summary of geotechnical characteristics of soil samples from Sandok and Shahkot landslides

No.	Sample ID.	Liquid limit	Plastic limit	Plasticity index	Specific gravity
Shahkot landslide					
1	SHKT-MS-(RF)	-	-	-	2.33
2	SHKT-MS-(M)	-	-	-	2.33
3	SHKT-MS-(LF)	-	-	-	2.59
4	SHKT-MB-(RF)	-	-	-	2.44
5	SHKT-MB-(M)	37.05	22.09	14.96	2.66
6	SHKT MB-(LF)	-	-	-	2.45
7	SHKT-TOE-(RF)	31.3	28.57	2.73	2.67
8	SHKT-TOE-(M)	26	23.95	2.05	2.72
9	SHKT-TOE-(LF)	23.9	21.75	2.15	2.45
Sandok landslide					
10	SDK-MB-(RF)	-	-	-	2.71
11	SDK-MB-(M)	38	31.52	6.48	2.53

**Table 3** Uniaxial compressive strength test results on rock cores from Shahkot and Sandok landslides

Sample ID	Dia of sample (mm)	Length of sample (Mm)	Area (mm <sup>2</sup> )	Failure load (kN)	Stress rate (kN/min)	UCS (MPa)
STS-1	47	94	1734.065	38.41	4.0	22.15
STS-2	47	94	1734.065	45.87	4.0	26.45
STS-3	47	94	1734.065	27.83	4.0	16.05
SJG-1	47	94	1734.065	71.50	4.0	41.23
SJG-2	47	94	1734.065	80.37	4.0	46.35
SJG-3	47	94	1734.065	78.40	4.0	45.21
SJG-4	47	94	1734.065	88.09	4.0	50.8
SJG-5	47	94	1734.065	80.98	4.0	46.7
SJG-6	47	94	1734.065	77.46	4.0	44.67
SJG-7	47	94	1734.065	87.62	4.0	50.53
SJG-8	47	94	1734.065	62.81	4.0	36.22
SJG-9	47	94	1734.065	67.98	4.0	39.2

STS stands for Shahkot Tanol schist

SJG stands for Sandok Jura granite

In hand specimen, the fresh surface of granite is light grey or whitish grey, while on the weathered surface, it appears yellowish grey or brownish black. Apart from feldspar, the main minerals seen in the hand specimen include muscovite, biotite, and quartz with minor amount of tourmaline and hornblende. Mineralogically, the granite is composed of quartz 40–55%, plagioclase 10–20%, potash feldspar 10–20%, muscovite 3–6%, biotite 2–4%, sericite 2–4%, opaque minerals 1–3%, and tourmaline 0–1% (Fig. 11b–d).

### Clay mineralogy of sliding surface material

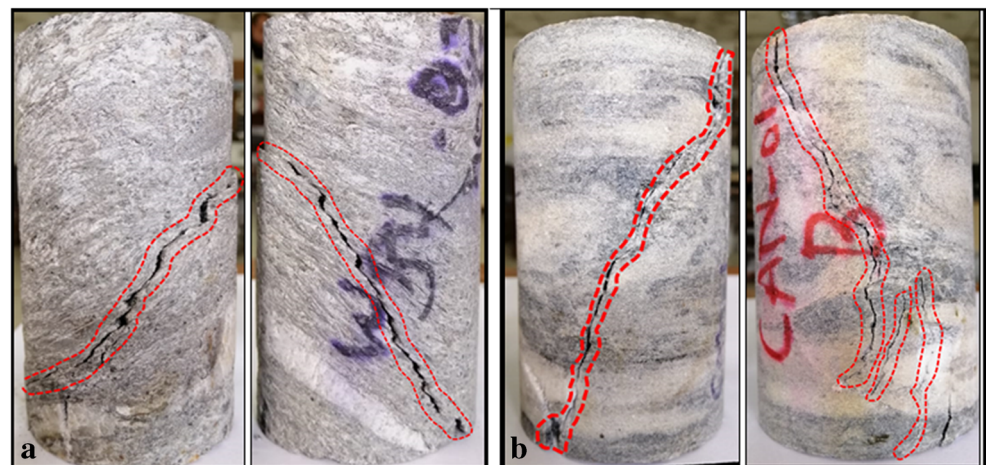
XRD technique was utilized in this study to establish bulk mineralogy of shale and clay of the Tanol Formation in the Shahkot landslide. The observed crystal lattice distance (d-spacing) in clays is correlated with joint committee on powder diffraction standard (JCPDS) for identification of different minerals. The results of XRD pattern presented in Fig. 12

indicate that the main constituted minerals present are quartz, muscovite, kaolinite, montmorillonite, illite, goethite, hematite, aragonite, siderite, calcite, dolomite, orthoclase, plagioclase, and gypsum. The results showed the presence of considerable amount of clay minerals montmorillonite, illite, and kaolinite. These minerals, specially montmorillonite, have greater swelling potential and increase the pore water pressure which is one of the causes of slope failure. The minerals like orthoclase and plagioclase are high-temperature minerals which are being chemically unstable and are more prone to chemical alteration. The other minerals like aragonite, calcite, and hematite also have greater affinity to weathering.

### Discussion

The presence of different types of landslides in the study area is because of the seismicity, intense rainfall, fragile nature of

**Fig. 10** **a** Failure mode observed on Tanol schist, failure along foliation planes; **b** Jura granite specimen under UCS; axial splitting and multiple fractured observed





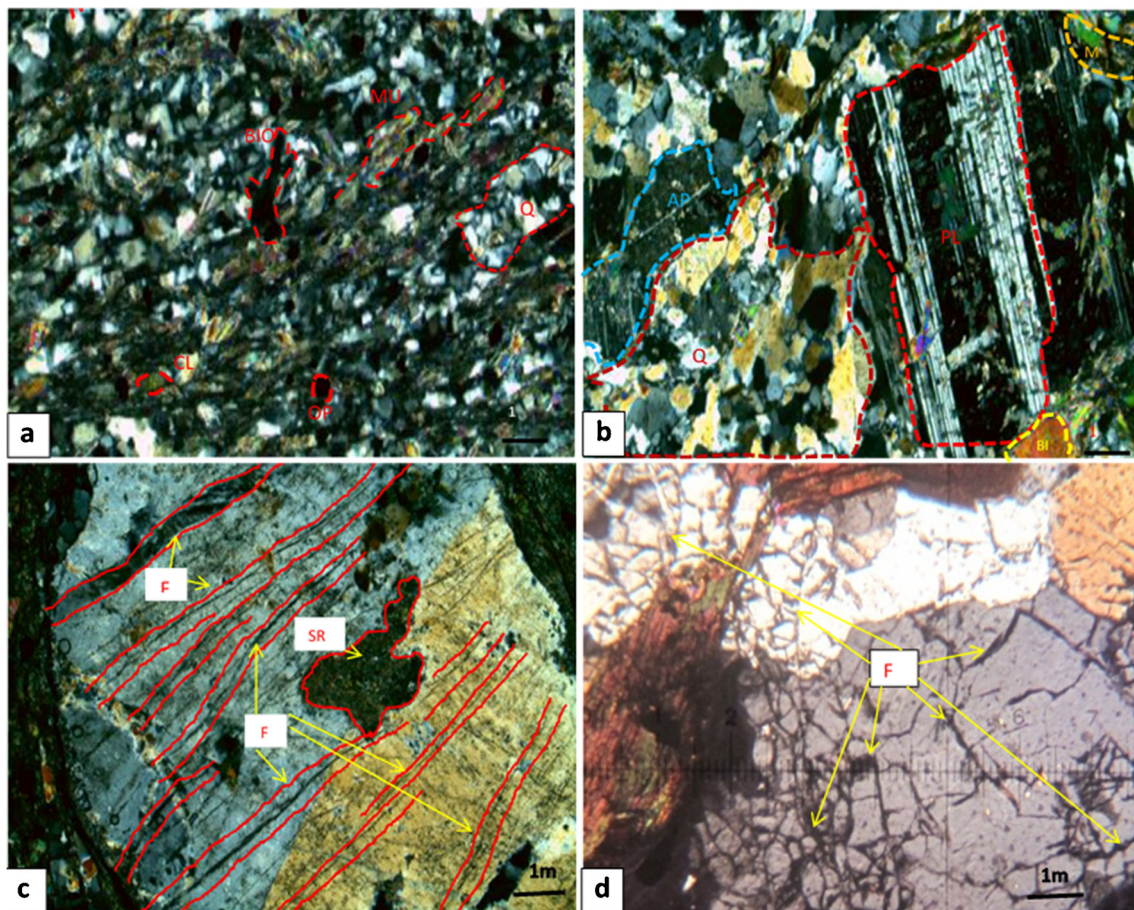


**Fig. 11** **a** Photomicrograph showing schist of Tanol Formation exposed in Shahkot landslide; Q quartz, MUC muscovite, BIO biotite, CL chlorite, OP opaque mineral (4x:xl); **b** photomicrograph showing Jura granite exposed in Sandok landslide. Q quartz, Pl plagioclase, AP altered plagioclase, MU muscovite, BIO biotite (4x:xl); **c** photomicrograph

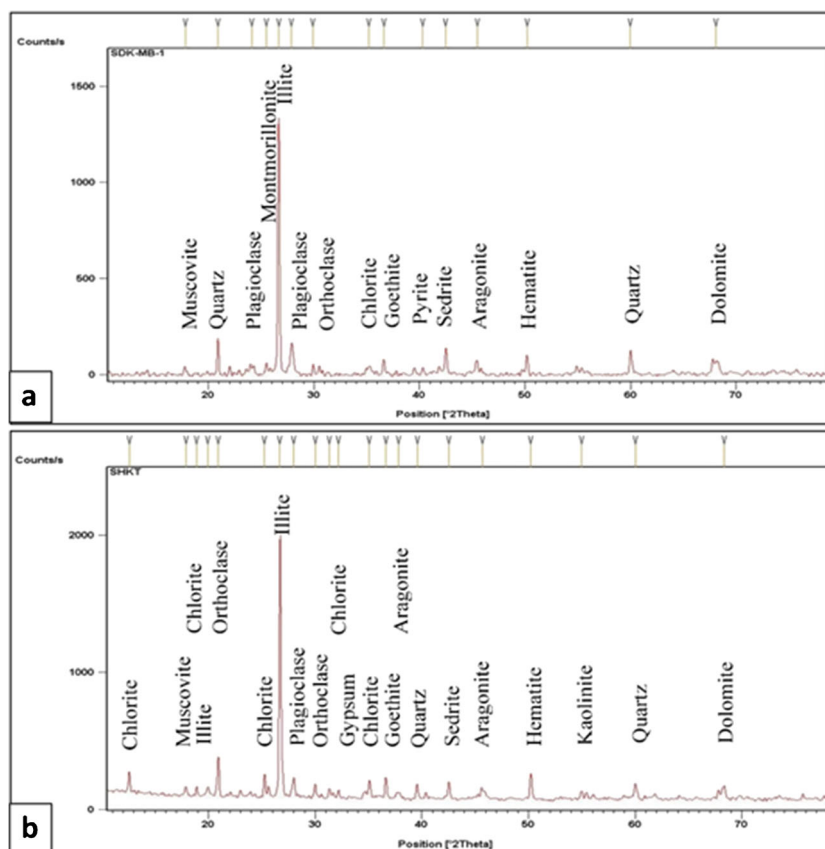
showing Jura granite exposed in Sandok landslide showing fractured feldspar crystal; FR fracture, SRT siricite (10x:xl); **d** photomicrograph showing Jura granite exposed in Sandok landslide showing multiple fractures in quartz crystals; FR fracture (10x:xl)

outcropping rocks, steep slopes, and narrow valley (Riaz et al. 2019). Multiple field visits found that about 74 landslides having different types occurred in the study area. Based on landslide susceptibility results, a problematic zone with a high frequency of landslide was selected for a more detailed investigation. Data-driven WoE method for landslide susceptibility analysis has been applied in landslide prone area, Lesser Himalayas, Pakistan. Contrary to the other studies, e.g., Lee and Choi (2004); Dahal et al. 2008) and Pradhan et al. (2010), weights were computed via Arc-SDM tool. Landslide susceptibility map integrating eight causative factors reveals that drainage network, faults, road network, and steep riverbed slopes are more prone for landslides in the studied area.

There are various factors that donate to the landslide susceptibility, e.g., lithological units, slope gradient, slope aspect, terrain elevation, landcover, discontinuity, and the location of roads and rivers. However, these causative factors vary from area to area, their effect is, to some extent, known, and have not revealed a great difference apart from lithology (El Jazouli et al. 2020).

A detailed field survey was carried out for two large-scale landslides. Detailed landslide mapping, profile drawings, and laboratory analysis such as geotechnical analysis, sieve analysis, Atterberg limits, specific gravity, UCS, and XRD analysis concluded that the Shahkot landslide is a rock and debris slide with slump failure towards the left flank. The sieve analysis, Atterberg limits, and specific gravity of disturbed soil sample suggest that the soils range from sandy, silty, and clay to gravel fraction which show cohesive, non-plastic to non-cohesive behavior. The PI indicates the occurrence of organic matter in the soil which has less impact on slope failure during rain fall or seepages. The UCS test values indicate high compressive strength of the material. The XRD analysis shows mineral composition of quartz, muscovite, kaolinite, goethite, aragonite, hematite, plagioclase, siderite, montmorillonite, calcite, gypsum, orthoclase, dolomite, and illite. Mechanical deformation is enhanced with richness of kaolinite, smectite, and illite having strong water absorption power. This study revealed that shear strength decreased with increasing

**Fig. 12** XRD analysis of Tanol Formation exposed in Shahkot landslide



moisture content, and hence, number of landslides increased relative to the particle size distribution of the clay. The Sandok landslide is a rockslide resulted by the failure of highly jointed and fractured granite. The sieve analysis, Atterberg limits, and specific gravity of disturbed soil sample suggest that the soil is non-cohesive with mainly clayey silty sand and gravels which is also supported by the XRD analysis showing higher concentration of clay mineral such as illite, which has higher swelling potential. The UCS test results show low compressive strength of granite, possibly reduced by previous seismic activities, presence of quartz filled veins, weathering effects, fracturing, and jointing in granite body experiencing freeze and thaw repeated episodes. Combining all analyses reveals that the Sandok granite is highly jointed and sheared which leads to the conclusion that this landslide occurred mainly due to fracture/joint failure in bed rock. Besides that, after the initial landslide episode, blasting method was applied to clear the road section which contributed in further fracturing of the granite body. The weight results of susceptibility mapping revealed that steep slopes, stream networks, lithological variations, and fault networks are the more influential factors for slope failure in the region. Geotechnical and geochemical analysis also support these results as weathered and crushed rocks having close proximity to faults revealed by low UCS, presence of clay minerals having swelling potential, and

abundant moisture provided by drainage network and rainwater percolations. Furthermore, undercutting by the river as well as anthropogenic activities along the steep slopes also increases the probability of slope failures.

## Conclusion

Landslide inventory mapping and classification were carried out, and subsequently, landslide susceptibility map was developed to document the most probable triggering factors along the studied road section. The Shahkot and the Sandok landslides in Athmuqam area along Neelum valley road were identified, first time documented, and classified as a debris slide-slump failure and rockslide, respectively. The possible causes of these landslides include steepness of slope, drainage network, existence of swelling clays and non-cohesive soils, intensive jointing and fracturing, repeated freeze and thaw episodes, seismic activities, river under cutting during flooding, and deforestation.

The sieve analysis, Atterberg limits, specific gravity, and XRD analysis of the disturbed soil sample and petrographic analysis show higher concentration of clay mineral such as montmorillonite, illite, and kaolinite which possess high swelling potential, show non-plastic to non-cohesive behavior



in case of Shahkot landslide. Very low UCS values of schist in Shahkot landslide indicate presence of flaky minerals and schistosity in relation to the failure planes. The UCS test results of the granite of Sandok landslide suggests the possible strength reduction by the presence of megascopic and microscopical fractures and joints produced as result of intense shearing along localized thrust faults and folds. Presence of calcite and quartz veins and repeated episodes of freeze and thaw action contributed to weathering and erosion. Gentle joint dip and open fractures are found in the scarp of the Sandok landslide and dip gently parallel to the escarpment slope. The landslide is probably advanced by stress release, freeze thaw, variations in moisture content, and creep movement. The disintegration affects the surface rocks to some extent, so that permeability and strength influenced badly at the weathered zone. The weaker zone shows the development of fracturing along the slope and finally slides due to heavy rainfall when it is immediately saturated or due to seismicity. Alternatively, these findings highlight the worth potential of landslide susceptibility analysis to identify the hazardous zones and geo-technical investigations and geochemical analysis to gain insight into the mineral compositions, rock strength, and moisture conditions which assumed the root cause of the landslide phenomenon.

**Acknowledgements** The authors are grateful to the Director Institute of Geology for providing transportation facilities during field work and Mr. Mudassir Shakeel for assisting in lab. work. Authors also express their sincere acknowledgements to Biswajeet Pradhan, Editor of the Arabian Journal of Geosciences and the two anonymous reviewers.

## Declarations

**Conflict of interest** The authors declare that they have no competing interests.

## References

- Akgun A (2012) A comparison of landslide susceptibility maps produced by logistic regression, multi-criteria decision, and likelihood ratio methods: a case study at İzmir, Turkey. *Landslides* 9(1):93–106
- Aleotti P, Chowdhury R (1999) Landslide hazard assessment: summary review and new perspectives. *Bull Eng Geol Environ* 58(1):21–44. <https://doi.org/10.1007/s100640050066>
- Ali SA, Parvin F, Vojteková J et al (2020) GIS-based landslide susceptibility modeling: a comparison between fuzzy multi-criteria and machine learning algorithms. *Geoscience Frontiers*
- Al-Najjar HH, Pradhan B (2020) Spatial landslide susceptibility assessment using machine learning techniques assisted by additional data created with generative adversarial networks. *Geosci Front* 12(2): 625–637
- Basharat M (2012) The distribution, characteristics and behavior of landslides triggered by the Kashmir Earthquake 2005, NW Himalaya, Pakistan, PhD thesis, University of Erlangen-Nuremberg, Germany, 186
- Basharat M, Rohn J, Baig MS, Ehret D (2012) Lithological and structural control of Hattian Bala rock avalanche triggered by the Kashmir earthquake 2005, NW Himalaya, Pakistan. *J Earth Sci* 23(2):213–224
- Basharat M, Rohn J, Baig MS, Khan MR, Schleier M (2014) Large scale landslides triggered by the Kashmir Earthquake 2005. *Pakistan J Mountain Science* 11(1):19–30
- Basharat M, Shah HR, Hameed N (2016) Landslide susceptibility mapping using GIS and weighted overlay method: a case study from NW Himalayas, Pakistan. *Arab J Geosci* 9(4):1–19
- Basharat M, Sarfraz Y, Ahmed KS et al (2017) A Preliminary investigation of reactivated mass movement near the epicenter of 2005 Kashmir earthquake, NW Himalayas, Pakistan. *Journal of Himalayan Earth Sciences* 50(1A):57–65
- Brabb EE (1984) Innovative approaches to landslide hazard mapping. In *Proc., 4th Int. Symp. On Landslides*, 307–324. Toronto
- Bragagnolo L, Silva RVD, Grzybowski JMV (2020) Artificial neural network ensembles applied to the mapping of landslide susceptibility. *Catena* 184:104240. <https://doi.org/10.1016/j.catena.2019.104240>
- Buša J, Tornyai R, Bednarik M et al (2019) Hodnotenie zosuvného hazardu pomocou multivariačnej a bivariačnej štatistickej analýzy v Košickej kotline (Západné Karpaty). *Geografický časopis* 71:383–405 (in Slovak with English abstract). [https://www.sav.sk/index.php?lang=en&doc=journallist&part=article\\_response\\_age&journal\\_article\\_no=17766](https://www.sav.sk/index.php?lang=en&doc=journallist&part=article_response_age&journal_article_no=17766)
- Calkins JA, Offield TW, Abdullah SKM et al (1975) Geology of the southern Himalaya in Hazara, Pakistan, and adjacent areas. *US Geol Surv Prof Pap*:716–c 29
- Can A, Dagdelenler G, Ercanoglu M, Sonmez H (2019) Landslide susceptibility mapping at Ovacik-Karabük (Turkey) using different artificial neural network models: comparison of training algorithms. *Bull Eng Geol Environ* 78(89):102–102. <https://doi.org/10.1007/s10064-017-1034-3>
- Chini M, Cinti FR, Stramondo S (2011) Co-seismic surface effects from very high-resolution panchromatic images: the case of the 2005 Kashmir (Pakistan) earthquake. *Nat Hazards Earth Syst Sci* 11: 931–943
- Dahal RK, Hasegawa S, Nonomura A, Yamanaka M, Masuda T, Nishino K (2008) GIS based weights-of-evidence modelling of rainfall-induced landslides in small catchments for landslide susceptibility mapping. *Environ Geol* 54(2):311–324. <https://doi.org/10.1007/s00254-007-0818-3>
- Dai FC, Lee CF (2001) Terrain-based mapping of landslide susceptibility using a geographical information system: a case study. *Can Geotech J* 38(5):911–923. <https://doi.org/10.1139/t01-021>
- Dunning SA, Mitchell WA, Rosser NJ, Petley DN (2007) The Hattian Bala rock avalanche and associated landslides triggered by the Kashmir earthquake of 8 October 2005. *Eng Geol* 93(3–4):130–144. <https://doi.org/10.1016/j.enggeo.2007.07.003>
- El Jazouli A, Barakat A, Khellouk R (2020) Geotechnical studies for landslide susceptibility in the high basin of the Oum Er Rbia river (Morocco). *Geology, Ecology, and Landscapes*:1–8
- Feizizadeh B, Roodposhti MS, Blaschke T, Aryal J (2017) Comparing GIS-based support vector machine kernel functions for landslide susceptibility mapping. *Arab J Geosci* 10:122. <https://doi.org/10.1007/s12517-017-2918-z>
- Fell R, Corominas J, Bonnard C, Cascini L, Leroi E, Savage WZ (2008) Guidelines for landslide susceptibility, hazard and risk zoning for land use planning. *Eng Geol* 102(34):85–98. <https://doi.org/10.1016/j.enggeo.2008.03.022>
- Ghazanfar M, Baig MS, Chaudhry MN (1983) Geology of Tithwal Kel area Neelum Valley, Azad Jammu and Kashmir. *Kashmir J Geol* 1: 1–10
- Guzzetti F, Reichenbach P, Cardinali M, Galli M, Ardizzone F (2005) Probabilistic landslide hazard assessment at the basin scale.

- Geomorphology 72(1–4):272–299. <https://doi.org/10.1016/j.geomorph.2005.06.002>
- Jadoon IAK, Hinderer M, Kausar AB, Qureshi AA, Baig MS, Basharat M, Frisch W (2015) Structural interpretation and geo-hazard assessment of a locking line: 2005 Kashmir Earthquake, western Himalayas. *Environ Earth Sci* 73:7587–7602. <https://doi.org/10.1007/s12665-0143929-7>
- Kalantar B, Pradhan B, Amir Naghibi S et al (2018) Assessment of the effects of training data selection on the landslide susceptibility mapping: a comparison between support vector machine (SVM), logistic regression (LR) and artificial neural networks (ANN). *Geomatics, Natural Hazards and Risk* 9:49–69. <https://doi.org/10.1080/19475705.2017.1407368>
- Kamp UB, Growley J, Khattak GA, Owen LA (2008) GIS-based landslide susceptibility mapping for the 2005 Kashmir earthquake region. *Geomorphol.* 101(4):631–642
- Kavzoglu T, Colkese I, Sahin EK (2019) Machine learning techniques in landslide susceptibility mapping: a survey and a case study. In: Pradhan S, Vishal V, Singh T (eds) *Landslides: theory, practice and modelling*. *Advances in Natural and Technological Hazards Research*, vol 50. Springer, Cham, pp 283–301. [https://doi.org/10.1007/978-3-319-77377-3\\_13](https://doi.org/10.1007/978-3-319-77377-3_13)
- Kazmi AH, Jan MQ (1997) *Geology and tectonics of Pakistan*, 557. Graphic Publishers, Karachi, Pakistan
- Khan MS (1994) Petrology and geochemistry of the Panjal volcanic in the Azad Kashmir and Kaghan areas of the NW Himalaya. Ph.D. dissertation, Univ. of Punjab
- Khan KP, Mohanty S, Mohanty M (2010) Geodynamics response of 8 October 2005 North Pakistan earthquake. *Geophys Surv* 31(1):85–106. <https://doi.org/10.1007/s10712-009-9083-1>
- Kiyota T, Sattar A, Konagai K, Kazmi ZA, Okuno D, Ikeda T (2011) Breaching failure of a huge landslide dam formed by the 2005 Kashmir earthquake. *Soils Found* 51(6):1179–1190
- Konagai K, Sattar A (2012) Partial breaching of Hattian Bala landslide dam formed in the 8<sup>th</sup> October 2005 Kashmir earthquake, Pakistan. *Landslides* 9(1):1–11
- Kumar KV, Martha TR, Roy PS (2006) Mapping damage in the Jammu and Kashmir caused by 8 October 2005 Mw 7.3 earthquake from the Cartosat-1 and Resourcesat-1 imagery. *Int J Remote Sens* 27(20):4449–4459. <https://doi.org/10.1080/01431160600702376>
- Lee S, Choi J (2004) Landslide susceptibility mapping using GIS and the weight of evidence model. *Int J Geogr Inf Sci* 18(8):789–814. <https://doi.org/10.1080/13658810410001702003>
- Lee S, Lee MJ, Jung HS (2017) Data mining approaches for landslide susceptibility mapping in Umyeonsan, Seoul, South Korea. *Appl Sci* 7(7):683. <https://doi.org/10.3390/app7070683>
- Leonardi G, Palamara R, Cirianni F (2016) Landslide susceptibility mapping using a fuzzy approach. *Procedia Eng* 161:380–387. <https://doi.org/10.1016/j.proeng.2016.08.578>
- Mahmood I, Qureshi SN, Tariq S, Atique L, Iqbal MF (2015) Analysis of landslides triggered by October 2005, Kashmir Earthquake. *PLoS Curr Disasters*:1–7. <https://doi.org/10.1371/currents.dis.0bc3ebc5b8adf5c7fe9fd3d702d44a99>
- Mittal S, Singh M, Kapur P et al (2008) Design and development of instrumentation network for landslide monitoring and issue an early warning. *J Sci Ind Res* 67(5):361
- Nefeslioglu HA, Gokceoglu C, Sonmez H (2008) An assessment on the use of logistic regression and artificial neural networks with different sampling strategies for the preparation of landslide susceptibility maps. *Eng Geol* 97(3):171–191. <https://doi.org/10.1016/j.enggeo.2008.01.004>
- Owen LA, Kamp U, Khattak GA, Harp EL, Keefer DK, Bauer MA (2008) Landslides triggered by the October 8, 2005, Kashmir earthquake. *Geomorphology* 94:1–9
- Petley D, Dunning S, Rosser N, Kausar AB (2006) Incipient landslides in the Jhelum Valley, Pakistan following the 8th October 2005 earthquake. *Disaster Mitigation of Rock Flows, Slope failures and Landslides* by Universal Academy Press:1–9
- Planning and Development Department AJK (2015) Geological mapping of Azad Jammu and Kashmir. No paging.
- Pradhan B, Lee S (2010) Delineation of landslide hazard areas on Penang Island, Malaysia, by using frequency ratio, logistic regression, and artificial neural network models. *Environ Earth Sci* 60:1037–1054
- Pradhan B, Oh JH, Buchroithner M (2010) Use of remote sensing data and GIS to produce a landslide susceptibility map of a landslide prone area using a weight of evidence model. *Remote Sensing Science Center for Cultural Heritage*:395–402
- Riaz MT, Basharat M, Hameed N, Shafique M, Luo J (2018) A data-driven approach to landslide-susceptibility mapping in mountainous terrain: case study from the Northwest Himalayas, Pakistan. *Natural Hazards Review* 19(4):05018007
- Riaz S, Wang G, Basharat M, Takara K (2019) Experimental investigation of a catastrophic landslide in northern Pakistan. *Landslides* 16(10):2017–2032
- Rieux SK, Qureshi RA, Peduzzi P et al (2007) An interdisciplinary approach to understanding landslides and risk management: a case study from earthquake affected Kashmir. In *Proc., Mountain Forum, Mountain GIS Conf*
- Saba SB, Meijde VDM, Werff HVD (2010) Spatiotemporal landslide detection for the 2005 Kashmir earthquake region. *Geomorphology* 124(1–2):17–25. <https://doi.org/10.1016/j.geomorph.2010.07.026>
- Sato PH, Hasegawa H, Fujiwara S et al (2007) Interpretation of landslide distribution triggered by the 2005 northern Pakistan earthquake using SPOT 5 imagery. *Landslides* 4(2):113–122. <https://doi.org/10.1007/s10346-0060069-5>
- Sattar A, Konagai K, Kiyota T, Ikeda T, Johansson J (2011) Measurement of debris mass changes and assessment of the dam-break flood potential of earthquake-triggered Hattian landslide dam. *Landslides* 8(2):171–182
- Senouci R, Taibi NE, Teodoro AC, Duarte L, Mansour H, Yahia Meddah R (2021) GIS-based expert knowledge for landslide susceptibility mapping (LSM): case of Mostaganem Coast District, West of Algeria. *Sustainability* 13(2):630
- Shafique M, Meijde MVD, Khan MA (2016) A review of the 2005 Kashmir earthquake-induced landslides; from remote sensing perspective. *J Asian Earth Sci* 118(Mar):68–80. <https://doi.org/10.1016/j.jseas.2016.01.002>
- Soeters R, Van Westen CJ (1996) In: Turner AK, Schuster RL (eds) *Slope instability recognition, analysis, and zonation*. In *Landslides-investigation and mitigation*. National Research Council, Washington, DC, pp 129–177
- Sujatha ER, Kumarave P, Rajamanickam V (2012) Landslide susceptibility mapping using remotely sensed data through conditional probability analysis using seed cell and point sampling techniques. *J Ind Soc Remote Sens* 40(4):669–678
- Van Westen CJ, Rengers N, Terlien MT, Soeters R (1997) Prediction of the occurrence of slope instability phenomena through GIS-based hazard zonation. *Geol Rundsch* 86(2):404–414. <https://doi.org/10.1007/s005310050149>
- Varnes DJ (1978) Slope movement type and processes. In: Schuster RL, Krizek RJ (eds) *Landslides: analysis and control*. National Academy of Sciences, vol 76. Transportation Research Board Special report, pp 12–33
- Vijith H, Madhu G (2008) Estimating potential landslide sites of an upland sub-watershed in Western Ghat's of Kerala (India) through frequency ratio and GIS. *Environ Geol* 55(7):1397–1405. <https://doi.org/10.1007/s00254-007-1090-2>
- Vojteková J, Vojtek M (2020) Assessment of landslide susceptibility at a local spatial scale applying the multi-criteria analysis and GIS: a case study from Slovakia. *Geom Nat Hazards Risk* 11(1):131–148

- Wadia DN (1931) The syntaxis of the north–west Himalaya-its rocks, tectonics, and orogeny. *Geol., Surv. India* 65:189–220
- Yalcin A (2008) GIS-based landslide susceptibility mapping using analytical hierarchy process and bivariate statistics in Ardesen (Turkey): comparison of results and confirmations. *Catena* 72(1):1–12. <https://doi.org/10.1016/j.catena.2007.01.003>
- Yilmaz I (2009) Landslide susceptibility mapping using frequency ratio, logistic regression, artificial neural networks and their comparison: a case study from Kat landslides (Tokat-Turkey). *Comput Geosci* 35(6):1125–1138
- Yilmaz I, Ercanoglu M (2019) Landslide inventory, sampling and effect of sampling strategies on landslide susceptibility/hazard modelling at a glance. In: Pourghasemi, H., Rossi, M. (Eds.), *Natural hazards GIS-based spatial modeling using data mining techniques. Advances in Natural and Technological Hazards Research*, vol 48. Springer, Cham. [https://doi.org/10.1007/978-3-319-73383-8\\_9](https://doi.org/10.1007/978-3-319-73383-8_9)
- Zhang TY, Han L, Zhang H, Zhao YH, Li XA, Zhao L (2019) GIS-based landslide susceptibility mapping using hybrid integration approaches of fractal dimension with index of entropy and support vector machine. *J Mt Sci* 16:1275–1288. <https://doi.org/10.1007/s11629-018-5337-z>